Front. Struct. Civ. Eng. 2023, 17(2): 238–255
https://doi.org/10.1007/s11709-022-0898-x

RESEARCH ARTICLE

Development and road performance of clear asphalt with high transparency and adhesion

Runhua GUO, Siquan LIU*

School of Civil Engineering, Tsinghua University, Beijing 100084, China
**Corresponding author. E-mail: liusq20@mails.tsinghua.edu.cn*

ABSTRACT Clear asphalt (CA) currently used in light-colored asphalt mixtures (LCAM) exhibits poor transparency and adhesion. Therefore, a highly transparent CA (HCA) modified using a silane coupling agent (KH550) was prepared. Furthermore, LCAM was prepared by mixing CA and limestone aggregates. The properties of the HCA and ordinary CA (OCA) were characterized using conventional asphalt tests, optical tests, pull-off tests, ultraviolet aging tests, dynamic shear rheometry, Fourier-transform infrared spectroscopy, differential scanning calorimetry, and scanning electron microscopy. Whereas Marshall, moisture resistance, wheel tracking, trabecular bending, and British pendulum tests were employed for the LCAM. The transmittance and spectral reflectance of the HCA were 123.30 and 3.74 times greater than those of the OCA, respectively. The complex modulus and viscosity-aging index of the HCA were 48% and 53% less than those of the OCA, respectively. After modification with KH550, the Marshall stability ratio, tensile strength ratio, and flexural strain of the HCA-prepared LCAM increased by 12.92%, 25.06%, and 23.90%, respectively. However, the rutting resistance of the HCA-prepared LCAM was 14.3% less than that of the OCA-prepared LCAM. The comprehensive performances of the HCA and HCA-prepared LCAM were 49.2% and 10.3% greater than those of the OCA and OCA-prepared LCAM, respectively, indicating a high application value in the future.

KEYWORDS light-colored asphalt pavement, orthogonal test, road performance, spectral reflectance, silane-coupling agent

1 Introduction

In recent years, increasing awareness of environmental problems and transportation safety has led to increased interest in nonblack asphalt pavement [1]. Light-color asphalt mixture (LCAM) is an important nonblack asphalt pavement material that uses clear asphalt (CA) instead of black asphalt to cover and bind the aggregates. A traditional black asphalt pavement is considered to be one of the main sources of temperature increase, whereas the high reflectivity of LCAM prevents pavement overheating during summer, which mitigates the urban heat island (UHI) effect and pavement distress [2]. The utilization of CA enables the construction of pavement of any color, providing a colorful appearance, improving the quality of people's lives, and preventing driver fatigue. Without pigment addition, CA provides the natural color of the mineral aggregates and integrates roads into areas of natural landscape or historical and cultural importance [3]. Moreover, LCAM is used to improve road illumination and visibility on ramps, bridges, and tunnels, reducing the power consumption of electrical lighting and improving safety.

CA is a crucial material for LCAM preparation because it exhibits viscosity–temperature characteristics similar to those of traditional asphalt. In general, CA can be prepared using four methods: a) removing dark asphaltene from asphalt [4], b) producing synthetic polymer binders [5], c) blending resin with a special bio-oil [6], and d) blending resin with a mineral oil [7]. After asphaltene removal, a brown or dark color is preserved in asphalt. Asif and Ahmad [2] and Pasetto et al. [8] studied the rheological and color characteristics of a thermoplastic bicomponent resin and found that it exhibited low stiffness and poor heat stability. Moreover, thermoplastic bicomponent resins are expensive [9], which makes them

Article history: Received Apr 14, 2022; Accepted Aug 26, 2022

difficult to popularize on a large scale. Merusi and Giuliani [10] reported that bio-oil-based CA exhibited superior chromatic performance compared to asphalt derived from asphaltene extraction and synthetic binder. However, Petrukhina et al. [11] noted that the cost of bio-oil is high, and the unsaturated character of bio-oil and high oxygen content leads to the poor aging resistance of the CA. Compared to the first three CA's mentioned above, CA prepared using petroleum resin and mineral oil is convenient and easy to produce. The mineral oil used is mainly aromatic oil, which has been widely used in producing colored asphalt pavements.

Wu et al. [12] indicated that although CA with a high aromatic oil content can be used to produce colored asphalt by adding pigments, the color of the CA produced was dark green or dark brown, neither of which can achieve the transparency requirements of LCAM for CA. Studies on transparent mineral oil-based CA are limited, and to the best of our knowledge, no research paper has been published on this topic. Other patents [13,14] have proposed that naphthenic oil (NO) can be mixed with resin to prepare CA with a certain transparency; however, owing to the limitation of the mechanical properties, this CA is mainly used in the construction of landscape paving installed in public parks and pedestrian walkways. Moreover, the transparency of the CA is mainly determined based on visual appearance, which is highly subjective and exhibits large errors.

In addition to the transparency problem, Tang et al. [15] and Lee and Kim [16] reported moisture damage problems such as looseness and stripping as the common distresses of colored asphalt mixtures due to the poor adhesion between the CA and aggregates. To overcome this problem, Bocci and Bocci [17] used $CaCO_3$ to replace a part of the mineral powder to improve the moisture resistance of LCAM used in tunnels. Tang et al. [18] employed a nano-montmorillonite and titanate coupling agent for CA modification to improve the water stability of the asphalt mixtures. Yang et al. [19] utilized a silane-coupling agent (SCA) to modify the aggregates, which improved the adhesion between the CA and aggregates and the water stability of the asphalt mixture. However, in the aforementioned method, the inorganic anti-stripping agent exhibited poor dispersibility; moreover, the titanate coupling agent had a dark color, which reduced the light transmittance of the CA. In addition, the amount of SCA required to modify the aggregates is considerable and its cost is high. Thus, applying this method in practical engineering is difficult. The use of SCAs for asphalt modification can effectively avoid the aforementioned problems. SCAs are colorless and transparent liquids that do not influence the transparency of CA. They are used in modified asphalt in a limited amount and are easy to disperse. However, only limited studies have explored the use of SCAs for CA modifications.

In conclusion, the widely used mineral oil-based CA has poor transparency and adhesion, which limits the engineering applications of LCAM. CA produced with NO exhibits improved transparency yet exhibit insufficient mechanical properties. The method used to improve the moisture resistance of LCAM leads to poor dispersibility of the anti-stripping agent, reduced transparency of the CA, and high cost. Therefore, the adhesion between the CA and aggregates must be improved to improve CA transparency. Moreover, it must be ensured that the road performance of LCAM meets the performance requirements of motor vehicle lanes, which is of considerable importance for promoting the engineering application of LCAM.

In this study, a highly transparent CA (HCA) is prepared using NO, a C5 hydrogenated petroleum resin (C5), styrene-butadiene-styrene (SBS), a defoamer (DF), and an antioxidant (AO) using an orthogonal test; an SCA (KH550) is selected as the modifier to improve the HCA adhesion. The HCA performance is evaluated by conducting mechanical, optical, ultraviolet (UV) aging resistance, and microscopic tests and compared to ordinary CA (OCA) performance. To test the road performance changes of the LCAM before and after modification, the Marshall stability, water stability, high- and low-temperature performance, and friction of all the LCAM are determined through laboratory tests. Furthermore, the economic cost and comprehensive performance of the CA and LCAM are analyzed. The obtained results can aid in developing and optimizing high-performance CA and LCAM.

2 Materials and specimen preparation

2.1 Raw materials

2.1.1 Raw materials for clear asphalt

C5 produced by Shenzhen Jitian Chemical Co. Ltd was used as the base material in the synthesis of the HCA; the properties of the C5 are listed in Table 1. NO produced by Hebei Oujia Lubricating Oil Co. Ltd was used as the softening harmonic component; the properties of the NO are listed in Table 2. SBS was obtained from Shandong Yuhuang Chemical Co. Ltd; the main properties of the SBS are given in Table 3. The AO was Irganox B900, produced by BASF (China) Co. Ltd; the characteristics of AO are listed in Table 4. KH550 was obtained from Nanjing Chuangshi Chemical Additives Co. Ltd; the characteristics of KH550 are listed in Table 5. The DF was tributyl phosphate, produced by Dongguan Defeng Defoamer Co. Ltd; the characteristics of the DF are listed in Table 6. For the comparison of the partial properties, OCA (Shandong Kant Fumei Colour Asphalt Engineering

Co. Ltd) was employed; the basic properties of OCA are listed in Table 7.

Table 1 Properties of C5

property	technical requirement	measured value	test method
softening point (°C)	100 ± 5	103	GB2294
yellow color index (50% toluene solution)	3.50–5.99	3.85	GB/T 22295
viscosity (190 °C) (mPa·s)	≤ 250	233	HG/T 3660
bromine value (gBr/100 g)	≤ 3.00	0.53	GB/T 24138
acid value (mgKOH/g)	≤ 0.50	0.08	GB2895
ash (%)	≤ 0.002	0.002	GB2295

Table 2 Properties of NO

property	technical requirement	measure value	test method
density (20 °C) (kg/m^3)	test result	928.8	GB/T 1884
kinematic viscosity (100 ℃) (mm^2/s)	16–26	23.55	GB/T 265
flashing point (°C)	≥ 210	231	GB/T 3536
pour point (°C)	≤ 15	−4	GB/T 3535
aniline point (°C)	≤ 99	93.5	GB/T 262
acid value (mgKOH/g)	test result	0.0152	GB/T 4945
polycyclic aromatic hydrocarbon content (%)	< 3.0	2.7	NB/SH/T 0838

Table 3 Properties of SBS

property	specification	measure value
molecular	–	linear
styrene content (%)	–	31
specific gravity	ISO 2781	0.94
tensile strength at break (MPa)	ISO 37	33
shore hardness (A)	ISO 868	72
melt flow rate (g/10 min)	ISO 1133	< 1
elongation at break (%)	ISO 37	880

Table 4 Characteristics of AO

density (g/cm^3)	volatile (%)	ash (%)	solubility (20 °C, acetone) (%)	melting point (°C)
1.02	0.5	0.1	100	60

Table 5 Characteristics of KH550

density (g/cm^3)	melting point (°C)	boiling point (°C)	refractive index (nD)	solubility	acid-base property
0.946	−70	217	1.420	water-soluble	alkalinity

Table 6 Characteristics of DF

density (g/cm^3)	melting point (°C)	boiling point (°C)	refractive index (nD)	acid value (mgKOH/g)
0.978	−79	289	1.424	0.1

2.1.2 Aggregates and filler

The aggregate used in this study was limestone (LM). As indicated in Table 8, the fundamental properties of LM satisfy the specification (Chinese standard JTG E42-2005 [20]) requirements. Hydrated lime (Tables 9 and 10) and limestone powder (Tables 11 and 12) were used as mineral fillers; their technical performance indexes meet the technical requirements of the specifications [21]. Hydrated lime can improve the resistance against moisture and frost damage in asphalt mixtures.

Table 7 Basic properties of OCA used in this research

technical characteristic	requirement	test result	specification
penetration (25 °C,100 g, 5 s) (0.1 mm)	60–80	69	ASTM D5
ductility (15 °C，5 cm/min) (cm)	≥ 100	> 100	ASTM D113
ductility (10 °C，5 cm/min) (cm)	≥ 30	40	
softening point (°C)	≥ 46	48	ASTM D36

Table 8 Fundamental properties of LM

parameter measured	test value	specification
apparent specific gravity	2.646	> 2.5
percent of flat and elongated particles (%)	11.7	< 18
Los Angeles abrasion value (%)	18	≤ 28
crush value (%)	18.3	≤ 26
fine aggregate angularity (%)	43.6	≥ 30
sand equivalent	78	≥ 60
immersion expansion (%)	0	≤ 3

Table 9 Chemical properties of hydrated lime

LO·I	SO_3	Fe_2O_3	MgO	Al_2O_3	SiO_2	CaO
37	0.12	1	16	6	10	29

Table 10 Physical properties of hydrated lime

specific gravity	surface area (m^2/kg)	pass sieve no. 200 (0.075) (%)
2.65	247	100

Table 11 Chemical properties of limestone powder

LO·I	SO_3	Fe_2O_3	MgO	Al_2O_3	SiO_2	CaO
27	1.50	–	2.0	–	1.0	69

Table 12 Physical properties of limestone powder

specific gravity	surface area (m^2/kg)	pass sieve no. 200 (0.075) (%)
2.43	395	100

2.1.3 Gradation design

At present, the economic cost of CA is higher than that of traditional asphalt; therefore, LCAM can be used as a thin-layer overlay, which allows quick construction and can be paved directly onto new or existing pavements, thus reducing construction costs. Therefore, in this study, AC-10 gradation, indicated by the curve in Fig. 1, was used. Furthermore, hydrated lime was used to replace 50% of the mineral filler.

2.2 Specimen preparation

2.2.1 Preparation of highly transparent clear asphalt

(1) Preparation

First, C5, SBS, AO, and NO were added to the reactor and mixed thoroughly. The reactor was then heated in an oven at 150 °C for 20 min. Subsequently, the reactor was removed from the oven, and the mixture was stirred with a high-speed shear mixer at 5000 r·min^{-1} for 40 min at 150 °C. After stirring for 20 min, the reactor was filled with KH550. Stirring continued for an additional 40 min.

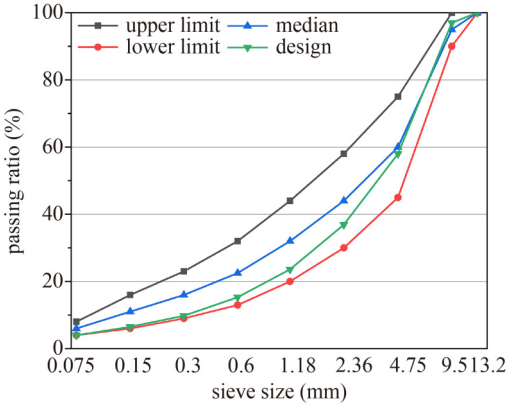

Fig. 1 Gradation curve of AC-10.

Then, DF was added and a glass stirring rod was used to mix the mixture at low speed. The reactor was then placed in a 150 °C oven for 1 h to eliminate the bubbles, indicating the successful synthesis of the HCA. The preparation process of the HCA is illustrated in Fig. 2. The color of the HCA is light and translucent amber, whereas that of OCA is dark green, as indicated in Fig. 3.

(2) Orthogonal test design

To quickly determine the optimal formula based on reducing the number of tests, the orthogonal test method was used in this study. The ratio of NO to C5 and the SBS and DF contents considerably influence the mechanical and optical performance of HCA. Therefore, in this orthogonal test, these three parameters were selected as the influencing factors, each of which was considered at three levels. To estimate the appropriate mass ratio of NO and C5 ($m_{NO} : m_{C5}$), the HCA was prepared by changing the mass fraction of the NO in the HCA without adding SBS; AO accounted for 2% of the total mass of the C5, with NO and DF at 0.5% of the total mass of the HCA. Conventional tests, including penetration (T 0605-2011), softening point (T 0606-2011), and ductility tests at 10 °C (T 0605-2011) were conducted according to Chinese Specification JTE E20-2011 [22]. As indicated in Fig. 4, the softening point and penetration of the HCA decreased and increased, respectively, with increasing NO content. However, brittle fracture occurred in all of the specimens in the ductility at 10 °C test (Fig. 5).

Currently, CA is typically prepared according to the 70# matrix asphalt standard. The indicators of the HCA prepared in this study met the requirements of the 70# colored asphalt binder in Chinese Specification GB/T 32984-2016 [23]. Therefore, according to the penetration (60–80) and softening point (46) standards, the three levels of $m_{NO} : m_{C5}$ were 46:54, 48:52, and 50:50. Based on previous research, the SBS content was the mass fraction of the total mass of C5 and NO, which was

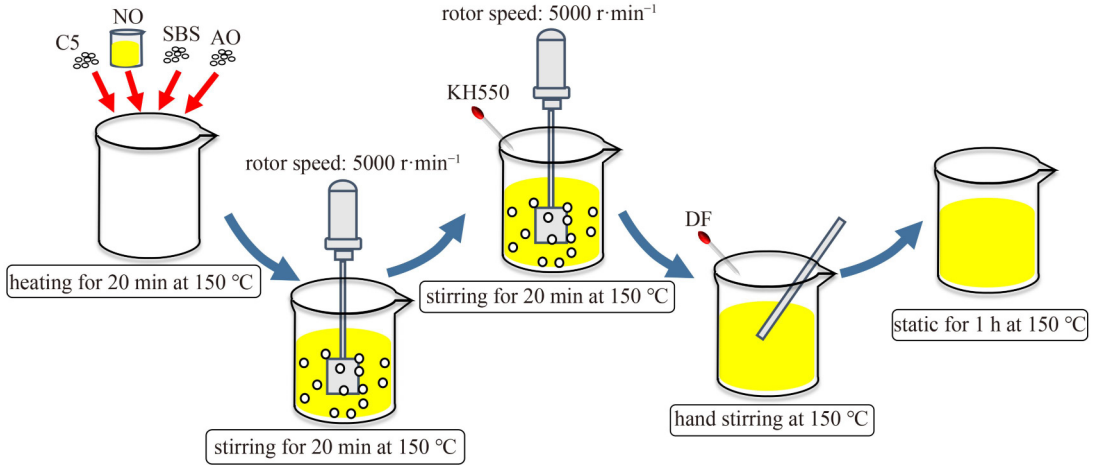

Fig. 2 Preparation process of HCA.

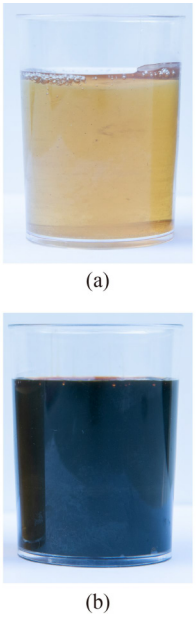

Fig. 3 Appearance display of: (a) HCA; (b) OCA.

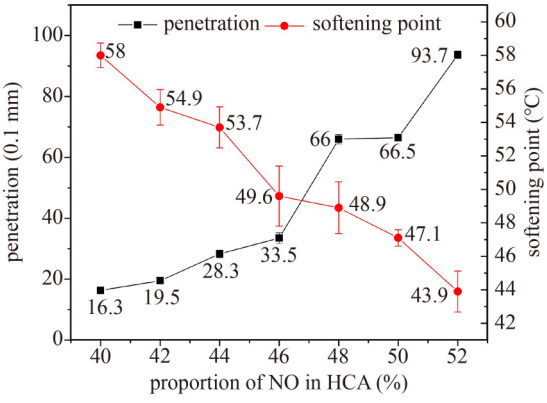

Fig. 4 Penetration and softening point of HCA with different NO content (error bars in the figure are standard deviations, unified throughout the text).

Fig. 5 Schematic diagram of brittle fracture of ductility at 10 °C specimens.

chosen as 4%, 5%, and 6% [24]. The DF content was the mass fraction of the total mass of the HCA, which was selected as 0.5%, 0.75%, and 1%. The three-factor and three-level orthogonal table is presented in Table 13.

2.2.2 Preparation of light-colored asphalt mixtures

For the LCAM preparation, the aggregates, limestone powder, hydrated lime, and CA were heated to 150 °C. Then, the heated aggregates were first mixed in a mixing pot preheated to 150 °C and then mixed with the HCA. After mixing for 90 s, hydrated lime and limestone powder were added and the mixture was mixed for 180 s to complete the preparation.

3 Experimental methods

3.1 Clear asphalt test

3.1.1 Optical test by spectrophotometer

Currently, a standard test method does not exist for the transmittance and solar spectral reflectance of CA. Therefore, in this study, CA flake samples were prepared with reference to the test methods for the transmittance and spectral reflectance of glass, film, and coatings. Accordingly, a spectrophotometer (LAMBDA950, PerkinEler) with a dual light source and scan range of 175–3300 nm was used for the test.

When preparing the CA test sample, an iron ring (50 mm × 50 mm × 4 mm, wall thickness of 1 mm) was placed on the test bench coated with the release agent. CA at 150 °C was poured into the iron ring after cooling to 25 °C, the sample was obtained (Fig. 6).

The sample was placed on a spectrophotometer holder and evaluated at a normal incidence angle of 0° during the transmittance test. The sample was placed at the center of the integrating sphere for the spectral reflectance test. Equations (1) and (2) were used to calculate the

Table 13 Design $L_9(3^3)$ orthogonal test scheme

scheme	$m_{NO} : m_{C5}$	SBS (%)	DF (%)
1	46 : 54	4	0.5
2	46 : 54	5	1
3	46 : 54	6	0.75
4	48 : 52	4	1
5	48 : 52	5	0.75
6	48 : 52	6	0.5
7	50 : 50	4	0.75
8	50 : 50	5	0.5
9	50 : 50	6	1

(a)

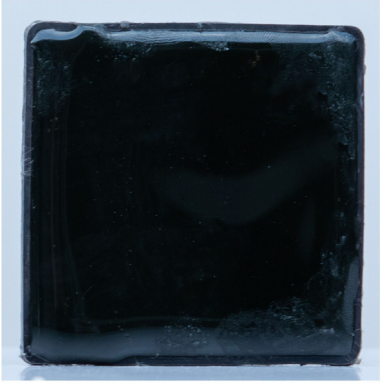

(b)

Fig. 6 Transmittance and spectral reflectance test samples of: (a) HCA; (b) OCA.

spectral reflectance of the CA samples at different wavelengths λ_i [25].

$$\rho = \frac{\sum_{i=1}^{n} \rho_{\lambda_i} E_s(\lambda) \Delta\lambda_i}{\sum_{i=1}^{n} E_s(\lambda) \Delta\lambda_i}, \tag{1}$$

$$\Delta\lambda_i = \frac{\lambda_{i+1} - \lambda_{i-1}}{2}, \tag{2}$$

where ρ represents the spectral reflectance, %; ρ_{λ_i} represents the spectral reflectance at wavelength λ_i, %; $E_s(\lambda)$ represents the solar spectral irradiance at wavelength λ_i (given in Table 1 of GB/T 17683.1 [26]), $W/(m^2 \cdot \mu m)$; $\Delta\lambda_i$ represents the wavelength interval, μm; and n denotes the number of test sites.

3.1.2 Pull-off test for clear asphalt

In accordance with AASHTO TP 91, the adhesion strength between the CA and aggregates was determined using the PosiTest AT instrument, as displayed in Fig. 7. The base material was smooth marble, which avoided texture and material effects on asphalt adhesion. Four parallel samples were prepared for each test group. After CA at 150 °C was dropped on the stone surface, the spindle was quickly placed on the asphalt surface. After the CA was cooled and the excess asphalt around the spindle removed, the test was conducted at 20 °C.

3.1.3 Static contact-angle test

A video optical contact-angle meter (OCA15Pro, Dataphysics) was used in this study. The CA samples were prepared by immersing the short sides of a rectangular glass in CA at 150 °C and then removing them. To obtain a flat CA coating, the slides were placed horizontally in a 150 °C oven for 30 min. The aggregate samples were cut into two parallel planes using a stonecutter, and the aggregate surfaces were smoothed with a polisher. Table 14 lists the surface free energy (SFE) components of the dropping solution, which was made from distilled water and ethylene glycol [27].

After obtaining the contact angle between the sample and test liquid, the polar and nonpolar parameters of the sample SFE could be calculated using Eq. (3) [28]. Furthermore, the adhesion work between the CA and aggregates could be calculated using Eq. (4).

$$\gamma_l(1 + \cos\theta) = 2\sqrt{\gamma_s^d \gamma_l^d} + 2\sqrt{\gamma_s^p \gamma_l^p}, \tag{3}$$

where γ_l, γ_l^d, and γ_l^p represent the SFE, nonpolar, and polar parameters of the test liquid, MJ/m^2; γ_s^p and γ_s^d represent the polar and nonpolar parameters of the samples, respectively, MJ/m^2; and θ represents the contact angle, °.

$$W_a = 2\sqrt{\gamma_{as}^d \gamma_{ag}^d} + 2\sqrt{\gamma_{as}^p \gamma_{ag}^p}, \tag{4}$$

where W_a represents the adhesion work between the CA and aggregates, MJ/m^2; γ_{as}^d and γ_{as}^p represent the nonpolar and polar parameters of the CA, MJ/m^2; and γ_{ag}^d and γ_{ag}^p represent the nonpolar and polar parameters of the aggregate, respectively, MJ/m^2.

Fig. 7 Pull-off test.

Table 14 SFE parameters (MJ/m^2) of test liquids

liquid	γ_l	γ_l^d	γ_l^p
distilled water	72.8	21.8	51
ethylene glycol	48	29	19

3.1.4 Ultraviolet aging test

The UV aging of the CA was performed in a UV aging box (Fig. 8) at a temperature of 60 °C; the UV radiation intensity on the specimen surfaces was 141 W/m^2. A total of 30 g of CA was placed in a round glass dish with diameter 15 cm. The thickness of the CA film was 1.5 mm. The indoor aging for 24 h was equivalent to exposure to outdoor ultraviolet radiation for two months [29]. The total UV aging time was 144 h, with portions of the samples removed every 48 h for testing.

3.1.5 Dynamic shear rheometer

Dynamic shear rheometer (DSR) (TA-AR1500EX, American) was employed to investigate the rheological properties of the CA under different UV aging times in accordance with AASHTO T 315 [30]. The strain-control mode was used with a strain value of 1% at a test frequency of 10 rad/s. Samples of 1-mm thickness were tested on a 25 mm plate. The temperature scan was conducted from 50 to 70 °C with a temperature increment of 5 °C per min.

3.1.6 Fourier-transform infrared spectroscopy test

The characteristic functional groups of the CA and raw materials were assessed by fourier-transform infrared (FTIR) spectroscopy. The presence of chemical reaction (s) during the CA synthesis was also analyzed. The wavenumber range was 400–4000 cm^{-1}, and the resolution was 2 cm^{-1}.

3.1.7 Differential scanning calorimeter test

A differential scanning calorimeter (DSC) (Q5000IR, TA INSTRUMENTS, China) was used to determine the glass transition temperature (T_g) and thermal stability of the CA. The weight of the CA sample was controlled at 5–10 mg. The heating scan ranged from –50 to 200 °C, with a heating rate of 10 °C/min in a nitrogen atmosphere.

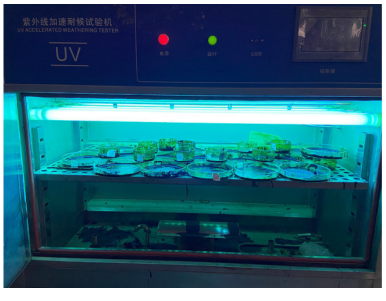

Fig. 8 UV aging box.

3.1.8 Microstructure analysis with scanning electron microscopy

Microstructure analysis with scanning electron microscopy (SEM) (JSM7401, Japan) was used to analyze the morphological properties of the HCA samples. The SEM had a resolution of 1.0 nm/1 kV and magnification range of 25 to 1000000 times. To prevent damage to the asphalt structure, the HCA was heated to 150 °C before being dropped on a 5 mm × 5 mm square silicon wafer; conductive double-sided tape was then applied to the CA sample. All samples were observed after gold spraying.

3.2 Light-colored asphalt mixtures test

3.2.1 Marshall test

The Marshall test was conducted according to the T 0709 test method in JTG E20-2011 [22]. The optimal CA content of the LCAM was determined by testing the strength and volume properties of the Marshall specimens. The specimens were placed in a water bath at 60 °C for 30–40 min before the Marshall stability and flow values were tested.

3.2.2 Moisture resistance test

The immersion Marshall stability and freeze-thaw cycle splitting tests were used to assess the water stability of the LCAM according to test methods T 0709-2011 and T 0729-2000 in JTG E20-2011 [22], respectively. The Marshall specimens were prepared and separated into two groups; the experimental group was placed in water at 60 °C for 48 h; the control group was immersed for 30 min at the same temperature. The Marshall stability ratio (*MSR*) was calculated using Eq. (5) to represent the water stability of the LCAM.

$$MSR = \frac{M_s}{M_d} \times 100\%, \tag{5}$$

where M_s and M_d represent the average stability of the specimens in the experimental and control groups, respectively, kN.

Eight Marshall specimens (50 compactions on each side) were randomly separated into two groups for the freeze-thaw cycle splitting test [22]. The specimens of the experimental group were soaked in water and evacuated at ambient temperature; then, they were frozen at –18 °C for 16 h. Subsequently, the specimens were soaked in water at 60 °C for 24 h. The specimens in the control group were maintained at 25 °C. Before testing, the two groups were placed in water at 25 °C for 2 h. The tensile strength ratio (*TSR*) was calculated using Eq. (6).

$$TSR = \frac{R_{T_2}}{R_{T_1}} \times 100\%, \quad (6)$$

where R_{T_1} and R_{T_2} represent the average tensile strengths of the specimens in the control and experimental groups, respectively, MPa.

3.2.3 Wheel tracking test

The assessment index for LCAM rutting resistance was dynamic stability (DS), which was determined by the wheel tracking test in accordance with test method T 0719-2011 in JTG E20-2011 [22]. DS was calculated using Eq. (7). The dimensions of the LCAM slab were 300 mm × 300 mm × 50 mm. The specimen was maintained at 60 °C for at least 5 h before testing. The wheel width used in the experiment was 50 mm, the pressure between the wheel and slab was 0.7 MPa, and the loading speed was 42 cycles/min.

$$DS = \frac{15N}{d_2 - d_1}, \quad (7)$$

where the DS units are cycles/mm; d_1, d_2 represent the vertical deformation depths at 45 and 60 min of testing, respectively, mm; and N represents the loading speed, fixed at 42 cycles/min.

3.2.4 Trabecular bending test

A trabecular bending test was performed to assess the fracture resistance of the LCAM at –10°C according to T 0715-2011 in JTG E20-2011 [22]. An LCAM slab with dimensions 300 mm × 300 mm × 50 mm was cut into beam specimens with dimensions 250 mm × 30 mm × 35 mm. The beam specimens were maintained at –10 °C for 5 h before testing. The specimens were subsequently tested on an MTS universal testing machine (E43.104) with a constant loading rate of 50 mm/min applied at the center. The crack-resistance assessment indexes of the LCAM were flexural strength and strain, which can be calculated using Eqs. (8) and (9).

$$R_B = \frac{3 \times L \times P_B}{2 \times b \times h^2}, \quad (8)$$

$$\varepsilon_B = \frac{6 \times h \times d}{L^2}, \quad (9)$$

where R_B represents the flexural tensile strength, MPa; ε_B represents the maximum bending tensile strain, $\mu\varepsilon$; b, h, and L represent the breadth, height, and length of the specimen, respectively, mm; P_B represents the peak load, N; and d represents the mid-length deflection when it fails, mm.

3.2.5 British pendulum test

The BM-III pendulum testing machine was employed to determine the skid resistance of the LCAM according to test method T 0964-2008 in JTG 3450−2019 [31]; each test included five repetitions. The measured result at room temperature (BPN_t) were converted to the standard value at 20 °C (BPN_{20}).

4 Results and discussion

4.1 Analysis of orthogonal design result

Table 15 lists the results of the orthogonal tests. Range analysis was used to determine the degree to which each factor influenced the experimental results; variance analysis was used to determine whether a certain factor significantly affected the experimental results. The results are presented in Table 16. The greater the range value in the range analysis, the greater the degree of the effect. Among the three indices, the range of $m_{NO} : m_{C5}$ was the largest, indicating that $m_{NO} : m_{C5}$ had the greatest effect on the high- and low-temperature properties and consistency

Table 15 Results of orthogonal test

scheme	penetration (0.1 mm)	softening point (°C)	ductility at 10 °C (cm)	transmittance (%)
1	33	74.8	59.3	17.97
2	42	77.9	80.4	7.10
3	54.6	80.3	128.5	3.12
4	64.2	74.6	132.5	2.33
5	74.2	73.7	134.9	13.59
6	54.5	77	130.9	18.93
7	99.3	71	135.5	3.36
8	101.5	73.4	134.6	0.48
9	91.1	75.3	135.6	33.2

Table 16 Range and variance analysis of orthogonal test results

factor	penetration (0.1 mm)			softening point (°C)			ductility at 10 °C (cm)			transmittance (%)		
	range	F	P	range	F	P	range	F	P	range	F	P
$m_{NO} : m_{C5}$	54.1	36.82	0.00	4.5	8.80	0.02	45.8	5.13	0.05	2.9	0.02	0.98
SBS content	7.1	0.71	0.53	4	7.49	0.02	22.6	1.02	0.42	11.3	0.41	0.68
DF content	13	2.34	0.18	0.9	0.48	0.64	24.7	1.23	0.36	7.5	0.16	0.86

of the HCA. For light transmittance, the range of the SBS was 8.4 and 3.8 times greater than those of the m_{NO} : m_{C5} and DF content, respectively, indicating that the SBS content had a significant effect on the light transmittance of the HCA.

In this study, the factors had two degrees of freedom and the errors had six degrees of freedom. When the F value exceeded the critical value $F_{0.05}$ (2, 6) = 5.14, and the P value was less than 0.05, the factor was regarded as having a considerable influence on the index value. Table 14 indicates that m_{NO} : m_{C5} had a significant effect on the consistency of the HCA, and that the m_{NO} : m_{C5} and SBS content had a significant effect on the high-temperature performance of the HCA. Based on the significance index, increasing the SBS content had minimal effect on the HCA penetration and ductility at 10 °C. However, unlike the preliminary test results in Subsection 2.2.1 (2), the ductility at 10°C increased significantly, indicating that the continual increase in SBS content had minimal effect on the performance of the CA in this instance. Because the P values of the DF content for all indicators and those of all factors for light transmittance were greater than 0.05, the effect of the DF content on performance and all factors on light transmittance was negligible. When m_{NO} : m_{C5} was 46:54 or 50:50, the HCA penetration index could not meet the index standard (60–80). Considering the orthogonal test results and economic factors, the formula for HCA was determined to be as follows: m_{NO} : m_{C5} = 48:52 + 4% SBS + 0.5% DF + 2% AO.

4.2 Effect of silane coupling agent on properties of clear asphalt

KH550 was used to modify the HCA in this study; HCA made based on the optimal formula was used as the control group. The three indexes of the HCA and the pull-off strength and adhesion work of the HCA and OCA were evaluated to reveal the influence of the KH550 on the HCA performance, determine the optimum content of KH550, and compare the adhesion of HCA and OCA. Figure 9 indicates that increasing the KH550 content increased the penetration of CA while decreasing the softening point. According to the ductility test performed at 10 °C, the ductility of all the samples was greater than 135 cm (the maximum range of the equipment) without fracture.

According to Fig. 10, the pull-off strength and adhesion work between the HCA and aggregates increased as the KH550 content increased. As indicated in Table 17, the surface energy of the HCA increased as the KH550 content increased; the greater the magnitude of the total SFE, the firmer the interface structure. These findings confirm that the use of KH550 increases the bonding characteristics of HCA and the aggregates. The pull-off strength and adhesion work of the OCA were less than those of the HCA at different KH550 contents, indicating that the adhesion between the HCA and aggregates was stronger than that of OCA. When the amount of KH550 exceeded 1%, the penetration index of the CA exceeded 80, which does not satisfy the penetration index standards of 70# color asphalt (60–80). The optimal dosage of KH550 was determined to be 1%.

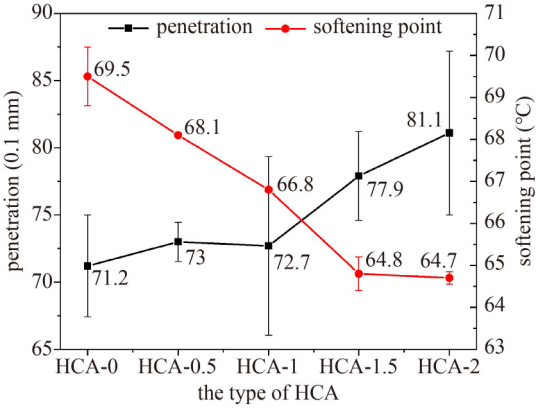

Fig. 9 Influence of KH550 content on penetration and softening point of HCA (HCA-*X* indicates that the mass fraction of KH550 in HCA is *X*%, unified throughout the text).

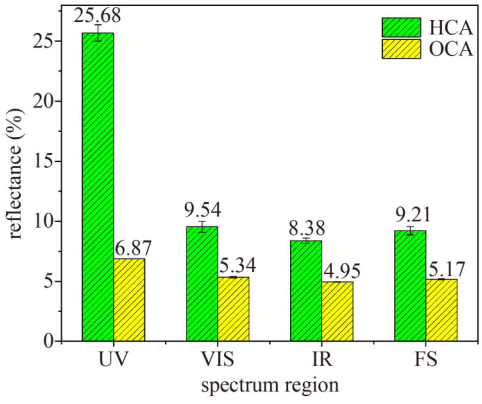

Fig. 10 Adhesion properties of CA.

Table 17 Contact angle and surface free energy parameters of samples

sample	contact angle (°)		SFE parameter (MJ/m^2)		
	distilled water	ethylene glycol	γ	γ^p	γ^d
HCA-0	103.4	83.7	16.41	2.16	14.25
HCA-0.5	101.2	81.0	17.61	2.51	15.10
HCA-1	97.8	76.2	20.13	2.93	17.20
HCA-1.5	97.6	73.9	22.39	2.28	20.11
HCA-2	95.6	71.4	23.58	2.65	20.93
OCA	102.7	77.6	22.61	0.90	21.71
LM	74.3	41.2	38.37	8.61	29.76

Note: γ, γ^d, and γ^p represent the SFE, non-polar, and polar parameters of test liquid, MJ/m^2.

4.3 Transmittance and spectral reflectance performance of clear asphalt

After determining the final formula of HCA (m_{NO} : m_{C5} = 48:52 + 4%SBS + 0.5%DF + 2%AO + 1%KH550), this study tested and compared the transmittance and spectral reflectance performances of the HCA and OCA. As displayed in Fig. 11, the transmittance of the HCA at each wave band was greater than that of the OCA. The average transmittance values at 580 nm for the HCA and OCA were 69.05% and 0.56%, respectively; the transmittance of the HCA was 123.30 times greater than that of the OCA, which indicates that the transparency of the HCA developed in this study was significantly improved compared to that of OCA.

The spectral reflectance of pavement materials is considered the main factor significantly influencing the UHI. The evaluated spectral reflectances of the HCA and OCA displayed in Fig. 12 indicate that the form and location of the reflectance spectrum curves of the two types of CA were significantly different. As indicated in Fig. 13, the spectral reflectance of the HCA decreased rapidly with the light's wavelength in the UV region. The visible (VIS) spectrum area exhibited an overshoot in the 409–514 nm range. There were three spectral reflectance fluctuation zones in the near-infrared (IR) region, 1100–1700 nm. HCA had a 3.74 times greater total spectral reflectance in the UV than in the OCA. Although UV light contributes only approximately 5% of solar energy, it is the main cause of aging or degradation of asphalt adhesives [32]; therefore, the HCA demonstrated superior UV aging resistance compared to the OCA. The total spectral reflectance of the HCA was 1.78 times that of the OCA. Compared to OCA, HCA had a greater spectral reflectance and produced a significant cooling effect.

4.4 Ultraviolet aging resistance of clear asphalt

The complex modulus-aging index (*CMAI*) and complex viscosities-aging index (*CVAI*) were used to assess the UV aging resistance of the CA; they can be calculated using Eqs. (10) and (11) [33]. In general, the UV aging of asphalt leads to an increase in the complex modulus and viscosity. Therefore, a lower *CMAI* and *CVAI* indicate superior CA aging resistance.

$$CMAI = \frac{G^*_{\text{aged}}}{G^*_{\text{unaged}}}, \tag{10}$$

$$CVAI = \frac{\eta^*_{\text{aged}}}{\eta^*_{\text{unaged}}}, \tag{11}$$

where G^*_{aged} is the complex modulus of the CA after UV aging, kPa; G^*_{unaged} is the complex modulus of CA before UV aging; η^*_{aged} is the complex viscosity of the CA after UV aging, Pa·s; and η^*_{unaged} is the complex viscosity of CA before UV aging.

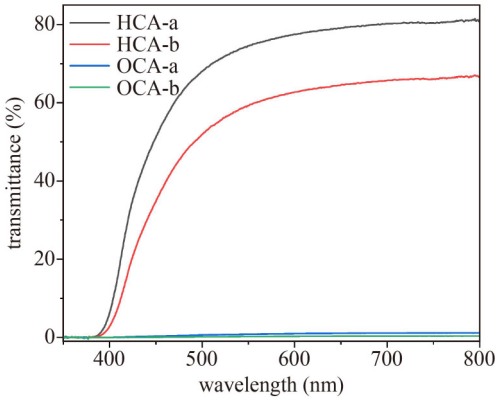

Fig. 11 Transmittance of HCA and OCA.

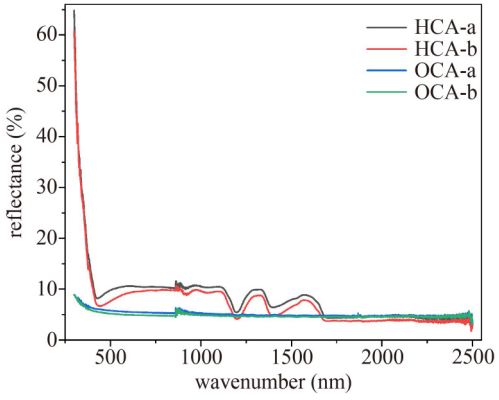

Fig. 12 Spectral reflectance curves of CA.

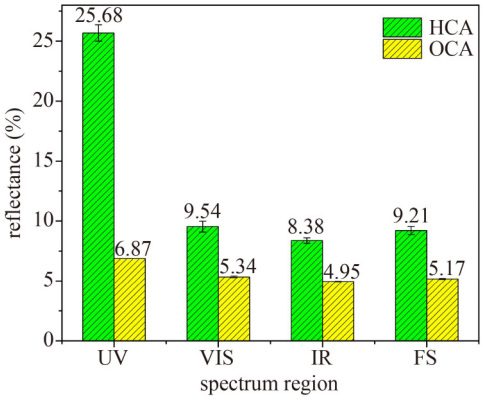

Fig. 13 Spectral reflectance of CA in different spectrum region.

Figure 14 displays the dynamic shear rheological characteristics of the CA at different UV aging times. The G^* values of the OCA and HCA increased after UV aging, indicating that UV aging improved the shear deformation resistance of the two types of CA. This is because UV aging causes the conversion of small molecules to larger molecules as well as the volatilization

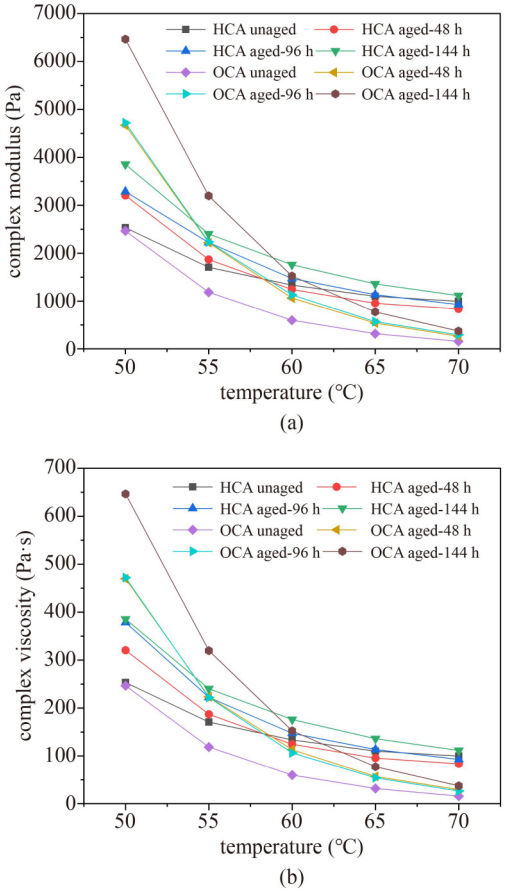

Fig. 14 Rheological properties of CA with different UV aging times: (a) complex modulus; (b) complex viscosity.

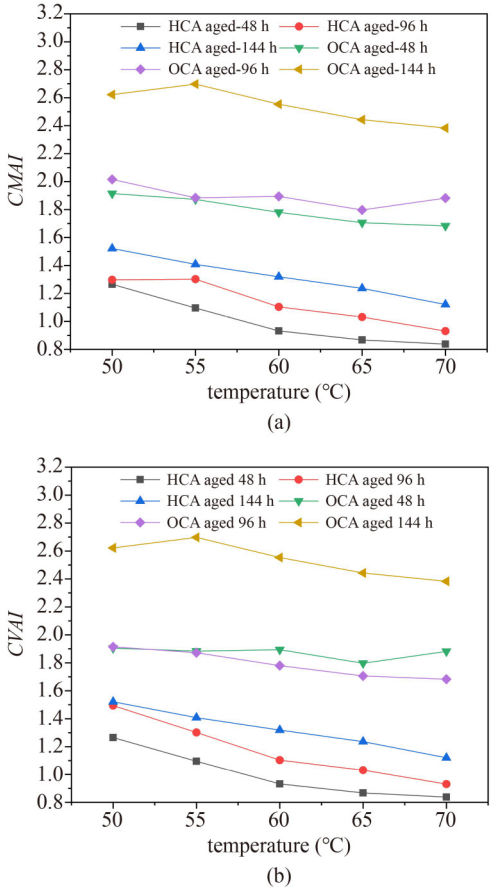

Fig. 15 Rheological aging indexes of CA with different aging times: (a) *CMAI* after UV aging; (b) *CVAI* after UV aging.

of light components in CA [34]. With an increase in aging time, the η^* of the HCA and OCA both increased gradually, indicating the hardening of the two types of CA during the UV aging process.

As indicated in Fig. 15, the *CMAI* and *CVAI* of the HCA and OCA both increased gradually with increasing aging time. Unlike OCA, HCA had a lower *CMAI* and *CVAI* in the sweep temperature range of 50 to 70 °C after UV aging for the same time. After UV aging for 144 h, the average *CMAI* of the HCA and OCA was 1.32 and 2.54, respectively; the average *CVAI* of the HCA and OCA was 1.12 and 2.38, respectively. The average *CMAI* and *CVAI* of the HCA were 48% and 53% less than those of the OCA, respectively, indicating that HCA had a greater UV aging resistance. The significant improvement in the UV resistance of the HCA comes primarily from two aspects: the total spectral reflectance of HCA in the UV is 3.74 times that of OCA based on Section 4.3, which effectively reduces the absorption of UV by the HCA; in the antioxidant B900, Irganox 1076 prevents further oxidation by retarding the carbonyl content growth [35], and Irgafos 168 allows hydrogen atoms to bind with the UV-excited reactive radicals and prevent further oxidation of the CA [36]. Both physical and chemical processes function to make HCA more effective in improving aging resistance compared to OCA.

4.5 Fourier-transform infrared spectroscopy

The results of the FTIR spectroscopy tests on NO, C5, SBS, KH550, AO, DF, and CA volatile residues are presented in Fig. 16. Unlike HCA, HCA_1 lacked both SBS and KH550 during preparation; HCA_2 lacked only KH550. As indicated in Fig. 16(a), compared to NO, C5, AO, and DF, the FTIR spectra of HCA_1 indicated no new absorption peaks. The C=C band at 1607 cm^{-1} in the FTIR spectra of NO was absent in that of HCA_1, which is because in the process of HCA_1 preparation, bond breakage occurred at 1607 cm^{-1} for the alkenes in the C5 and the unsaturated hydrocarbons of the NO transformed to alkanes during the HCA_1 production process [37]. These findings indicate that in the preparation of HCA_1, a physical mixing process and specific chemical reaction occur concurrently.

Comparing the FTIR spectra of HCA_1, SBS, and HCA_2 indicates that the SBS modifier characteristic bands at 698 and 963 cm^{-1} appeared in HCA_2. However, no new absorption peaks were observed, indicating that HCA_1

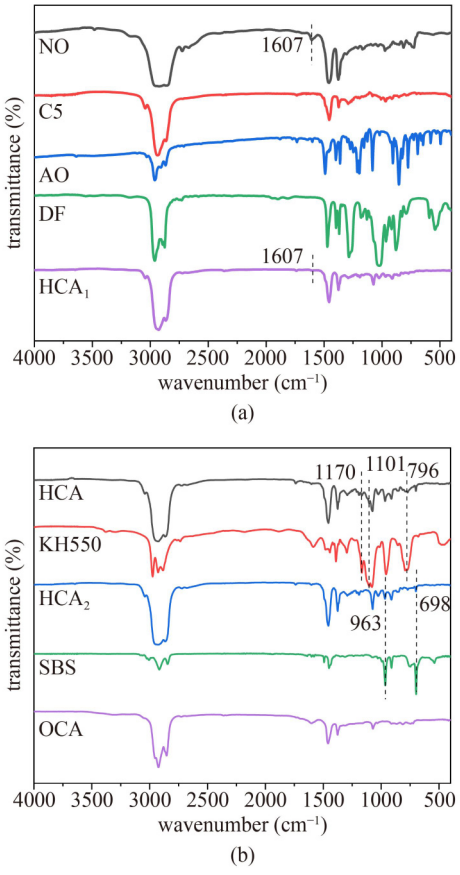

Fig. 16 FTIR spectra of: (a) raw materials and HCA_1; (b) HCA and OCA.

was physically modified by SBS. A comparison of the FTIR spectra of HCA_2, KH550, and HCA indicated that HCA has peaks matching KH550 at 796, 1101, and 1170 cm^{-1}, indicating that the HCA was modified by the KH550, although mainly by physical modification. The FTIR spectra of the HCA_1, HCA_2, and OCA were similar; that is, it can be concluded that the main functional groups of the HCA and OCA, which are composed of aromatic compounds and aliphatic carbon oxides containing a benzene ring structure, are the same [38]. The functional group composition of CA is similar to that of petroleum asphalt , which provides theoretical support for the use of HCA as a road material.

4.6 Differential scanning calorimeter results

T_g and thermal stability are important thermal properties of asphalts. DSC tests were performed on the samples to compare the thermal properties of the CA; the results are displayed in Fig. 17. Asphalt can be transformed from glassy to rubbery upon heating. The low-temperature performance of CA was assessed using T_g. A higher T_g indicates reduced low-temperature CA performance [39]. The T_g values of HCA and OCA were −28.06 and −20.86 °C, respectively, indicating that HCA has superior low-temperature performance compared to OCA. This explains why HCA demonstrated excellent ductility at 10 °C. The magnitude of enthalpy in the DSC curves was used to assess the thermal stability of the asphalt; the greater the enthalpy, the worse the thermal stability of the material [40]. The total enthalpy values of HCA and OCA were 0.75 and 15.07 J/g, respectively, indicating that the HCA had robust thermal stability.

4.7 Scanning electron microscopy analysis

The SEM images of the HCA without SBS and HCA modified with 4% SBS are displayed in Fig. 18. The results indicate that the HCA without SBS was a dense homogeneous structural system, and the surface was relatively smooth, except for a few folds. For the 4%

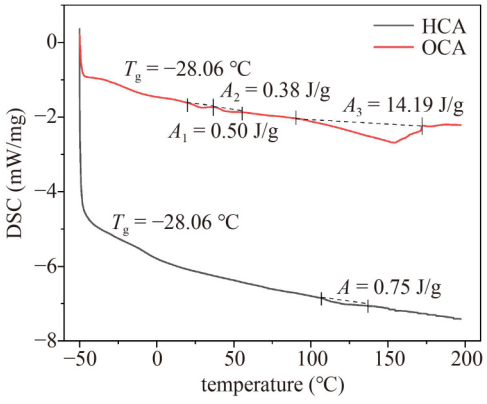

Fig. 17 DSC curves of CA.

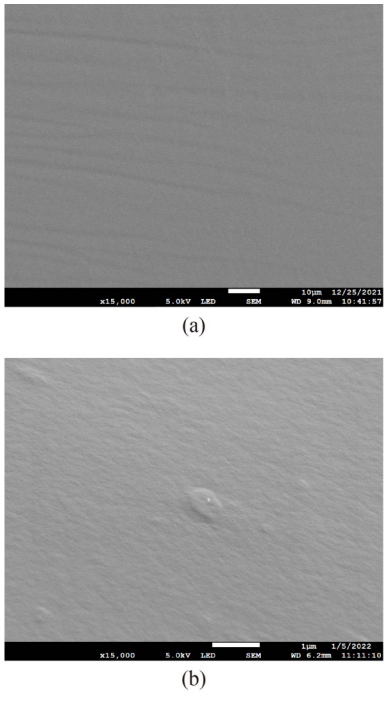

Fig. 18 SEM images of: (a) HCA without modification with SBS; (b) HCA modified by 4% SBS.

SBS-modified HCA, the SBS was cut into micron-sized particles that were evenly distributed and adsorbed in the asphalt. Each particle was coated and encircled with the bitumen medium, forming an acceptable bond with the bitumen. Numerous fluffy protrusions were formed on the surface of the substrate, and the asphalt contained numerous SBS segments and evenly dispersed particles. The phase interface layer of the two-phase structural system was created by the SBS particles and asphalt components adsorbed on the surface, resulting in a stable three-dimensional network structure [41]. This improved the ductility and elastoplasticity of the HCA, which explains why the HCA ductility improvement at 10 °C after modification with SBS was so apparent (compare the test results of Subsection 2.2.1(2) and 4.1).

4.8 Road performance of light-colored asphalt mixtures

4.8.1 Marshall test

Table 18 presents the Marshall test results, which meet the requirements of dense grade color asphalt concrete in accordance with Chinese Standard GB/T 32984-2016 [23]. Apparently, the optimum asphalt contents (OAC) of the LCAM specimens using different types of CA were similar. The Marshall stability of the HCA-1-prepared LCAM was 15.05% and 7.53% greater than those of the HCA-0-prepared LCAM and OCA-prepared LCAM, respectively, indicating that the Marshall stability of the LCAM was significantly enhanced and exceeded that of the LCAM prepared with OCA following KH550 modification.

4.8.2 Moisture resistance test

The water immersion Marshall stability and freeze-thaw splitting tests were used to obtain the *MSR* and *TSR* of the LCAM specimens prepared with different types of CA; the results are displayed in Fig. 19. As illustrated in Fig. 19(a), the *MSR* of the LCAM made with three types of CA all achieved the technical requirements (*MSR* ⩾ 80%) of the specifications for colored asphalt concrete applied to motor vehicle lanes [23]. The OCA-prepared LCAM had a lower *MSR* than the HCA-prepared LCAM. Compared to the HCA-0-prepared LCAM and OCA-prepared LCAM, the *MSR* of the HCA-1-prepared LCAM improved by 10.91% and 17.08%, respectively.

Table 18 Results obtained by the Marshall test for specimens of LCPM

CA type	OAC (%)	air-void content (%)	density (g/cm^3)	Marshall stability (kN)	flow (0.1 mm)
OCA	5.54	4.0	2.39	9.43	2.75
HCA-0	5.67	3.9	2.40	8.77	2.71
HCA-1	5.68	4.1	2.44	10.09	2.86

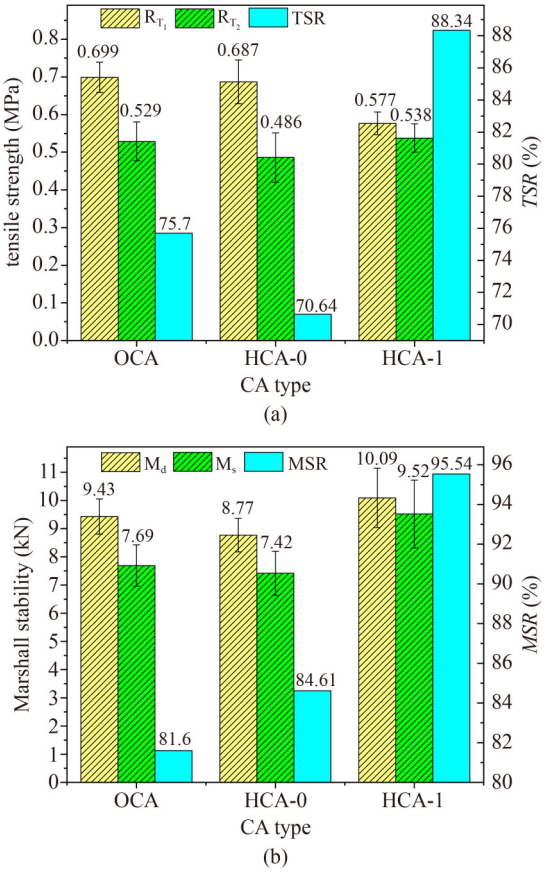

Fig. 19 Results of moisture resistance test: (a) water immersion Marshall stability test; (b) freeze–thaw cycle splitting test.

As indicated in Fig. 19(b), the *TSR* of the OCA-prepared LCAM and HCA-0-prepared LCAM was less than 80% and 75%, respectively, which does not satisfy the technical requirement of colored asphalt concrete applied to non-motor vehicle lanes. Only the HCA-1-prepared LCAM was greater than 80%, meeting the technical requirements of colored asphalt concrete applied to motor vehicle lanes [23]. The *TSR* of the LCAM increased by 25.06% and 16.90% after modification with KH550 compared to the HCA-0-prepared LCAM and OCA-prepared LCAM, respectively. The aforementioned findings demonstrate that KH550 considerably enhanced the water stability of the LCAM, which is compatible with the pull-off test and contact-angle test results.

4.8.3 High and low temperature performance

As indicated in Fig. 20(a), compared to the OCA-prepared LCAM, the DS of the HCA-prepared LCAM before and after modification with KH550 decreased by 7.2% and 14.3%, respectively. Apparently, the KH550 modification reduced the rutting resistance of the HCA-prepared LCAM, which is consistent with the changes in

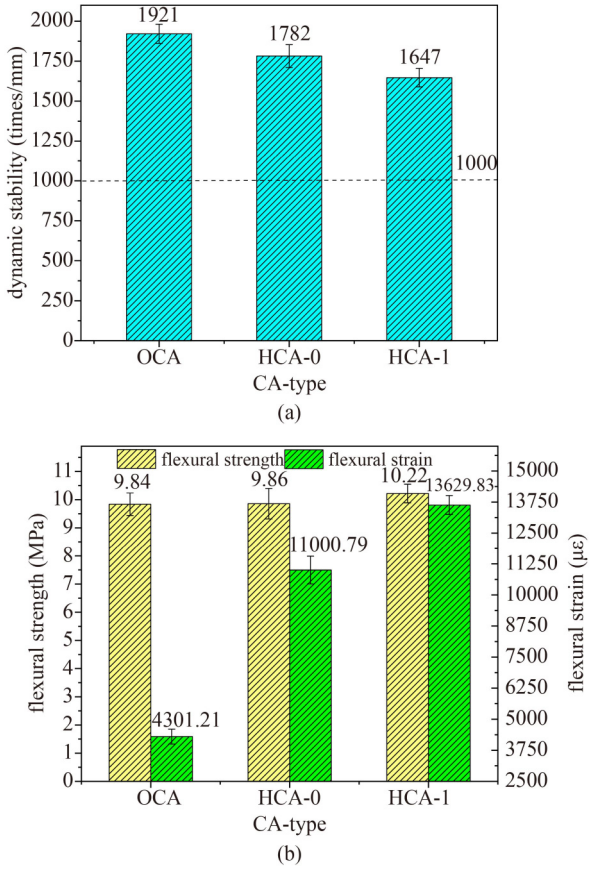

Fig. 20 The high and low temperature test results: (a) rutting test; (b) low-temperature bending test.

the penetration and softening point characteristics of the KH550-modified HCA. When KH550 was added to the HCA, part of the KH550 was coupled to the oil in the HCA, and the unbound coupling-agent molecule remained in the HCA, which had a diluting role, leading to a decrease in the asphalt consistency and weakening of the high-temperature stability. However, under this KH550 content, the dynamic stability of the LCAM continued to meet the engineering requirements (dynamic stability ⩾ 1000) [23].

The flexural strength and strain at failure of the LCAM specimens prepared with different types of CA were determined using a low-temperature trabecular bending test; the results are presented in Fig. 20(b). The low-temperature cracking resistance of the LCAM prepared from all three types of CA met the technical requirements of colored asphalt concrete applied to motor vehicle lanes (flexural strain ⩾ 2000) [23]. Both the flexural strength and strain of the HCA-prepared LCAM were greater than those of the OCA-prepared LCAM, with the improvement in flexural strain being the most noticeable. The flexural strain of the LCAM made using HCA before and after modification was 216.90% and 155.77% greater than that of the OCA-prepared LCAM, respectively. The low-temperature crack resistance increased marginally when the LCAM was modified with KH550, indicating that KH550 improved the low-temperature performance of the materials.

4.8.4 Skid resistance

The measurement was performed five times for each rutting slab measurement point, and the average results were calculated to represent the friction coefficient at this spot. The corrected BPN_{20} values of the LCAM prepared with different types of CA are displayed in Fig. 21. It can be observed that the BPN values of all LCAMs were greater than the specification requirement of 45 [42], and the values were relatively close, indicating that the CA-type did not influence the skid resistance of the LCAMs.

4.8.5 Comparison of highly transparent clear asphalt-prepared light-colored asphalt mixtures with conventional asphalt mixture and existing research

To further evaluate the mechanical properties of the developed LCAM, the road performance of the HCA-prepared LCAM was compared to that of the 70# matrix asphalt mixture and the results of the LCAM with the same gradation in this field. The results are presented in Table 19.

The road performance of the HCA-prepared LCAM satisfied the requirements of the 70# matrix asphalt mixture (Table 17). The *DS* and *MSR* of the HCA-prepared LCAM were marginally less than the results of Research A [19]; however, the flexural strain of the

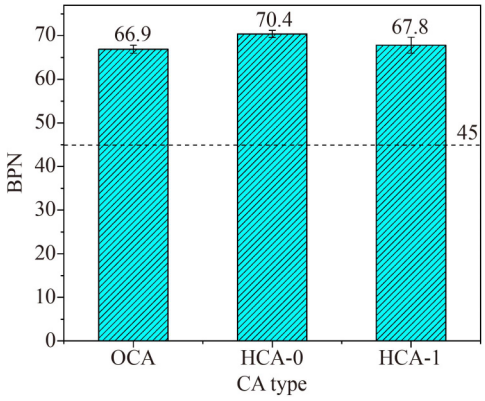

Fig. 21 BPN of LCAM.

Table 19 Results of comparison

item	*DS*	*MSR*	*TSR*	flexural strain
HCA-prepared LCAM	1647	95.54	88.34	13629.83
requirements of 70# matrix asphalt mixture [29]	⩾ 1000	⩾ 80	⩾ 75	⩾ 2600
Research A [19]	1649	96.6	–	1750
Research B [43]	825	94.2	93	3742

LCAM in Research A did not meet the technical requirements for either the colored asphalt concrete applied to motor vehicle lanes (flexural strain ⩾ 2000) [23] or the 70# matrix asphalt mixture in Table 17. The *TSR* of the HCA-prepared LCAM was 4.66% less than that of the LCAM presented in Research B; however, the other indices of the HCA-prepared LCAM were greater than the test results of Research B. The *DS* of the LCAM reported in Research B [43] did not meet either the technical requirements (*DS* ⩾ 1000) of colored asphalt concrete applied to motor vehicle lanes [23] or 70# matrix asphalt mixture in Table 17.

In summary, compared to the technical requirements of conventional asphalt and LCAM of the same gradation in the same field, the HCA-prepared LCAM exhibited acceptable road performance.

4.8.6 Analysis of economic costs and comprehensive performance

To evaluate the practical application value of the developed HCA and HCA-prepared LCAM, the economic cost and comprehensive performance were analyzed. Only the material costs were considered in the economic analysis. Table 20 presents the raw material costs required for the preparation of the HCA and LCAM. The cost per ton of HCA was 10.6% greater than that of the OCA.

According to the OAC obtained in Table 18 and the price provided in Table 20, it can be calculated that the cost of the OCA-prepared LCAM was \$285/m^3, and the cost of the HCA-prepared LCAM was approximately \$312/m^3. The cost increased by 9.5% because of the high production cost of HCA and the large amounts of OAC in the HCA-prepared LCAM.

Although the cost of the HCA-prepared LCAM increased, the high light transmittance of the HCA could expand the road function. Moreover, road performance, such as moisture resistance, was improved. To comprehensively evaluate the cost, road performance, and environmental benefits of HCA and the HCA-prepared LCAM, the efficacy coefficient method [44] was proposed to assess the comprehensive performance of HCA and HCA-prepared LCAM compared to OCA and OCA-prepared LCAM, respectively.

The representative performance indices of the CA and LCAM were selected as the evaluation indices. The coefficient of variation v_i and weight of the ith evaluation index were obtained using Eqs. (12) and (13), respectively [45]. The evaluation indices and data processing results are listed in Table 21.

$$v_i = \frac{\sigma_i}{\bar{X}_i}, \tag{12}$$

Table 20 Cost of materials

material	price (\$/t)	material	price (\$/t)
C5	1642	HCA	1403
NO	896	OCA	1269
SBS	2015	LM	52
KH550	4328	hydrated lime	101
AO	4328	limestone powder	67
DF	1194		

Note: 1 \$ = 6.7 RMB (reference on 2022).

Table 21 Evaluation indexes and data calculation results

evaluation indicator	X_{hi}	X_{si}	average value	variation coefficient	weight
transmittance (%)	69.05	0.56	34.81	0.98	0.2789
spectral reflectance (%)	9.21	5.17	7.19	0.28	0.0796
CMAI	1.32	2.54	1.93	0.61	0.0896
CVAI	1.12	2.38	1.75	0.63	0.1020
penetration (0.1 mm)	69	72.7	70.85	0.03	0.0074
softening point (°C)	66.8	48	57.40	0.16	0.0464
ductility (cm)	135	40	117.50	0.15	0.0422
pull-off strength (MPa)	0.2	0.147	0.17	0.15	0.0433
adhesion work (MJ/m^2)	62.55	53.22	57.89	0.08	0.0228
DS (cycles/mm)	1921	1647	1784.00	0.08	0.0096
MSR (%)	95.54	81.6	88.57	0.08	0.0218
TSR (%)	88.34	75.7	82.02	0.08	0.0223
flexural strain (με)	13629.83	4301.21	8965.52	0.52	0.0218
BPN	67.8	66.9	67.35	0.45	0.1475
cost of CA (\$/t)	1238.8	1567.2	1403.00	164.20	0.0019
cost of LCAM (\$/m^3)	285	312	10.05	1.05	0.0332

where v_i, σ_i, and $\bar{X}_i$ represent the coefficient of variation, standard deviation, and average value of the ith evaluation index, respectively.

$$\omega_i = \frac{v_i}{\sum_1^n v_i}, \tag{13}$$

where ω_i represents the weight of the ith evaluation index, $\sum_1^n v_i$ represents the sum of the coefficients for all evaluation indexes, and n represents the number of evaluation indexes.

The evaluation index includes extremely large and extremely small variables; the methods for determining the two variable types are displayed in Eqs. (14) and (15), respectively.

$$d_{1i} = \begin{cases} \dfrac{X_i - X_{si}}{X_{hi} - X_{si}} \times 0.4 + 0.6, & X_i < X_{hi}, \\ 1, & X_i \geqslant X_{hi}, \end{cases} \tag{14}$$

$$d_{2i} = \begin{cases} \dfrac{X_i - X_{si}}{X_{hi} - X_{si}} \times 0.4 + 0.6, & X_i > X_{si}, \\ 1, & X_i \leqslant X_{si}, \end{cases} \tag{15}$$

where d_{1i} and d_{2i} represent the single efficacy coefficient of the i-th extremely large and small evaluation index, respectively, and X_i, X_{hi}, and X_{si} represent the actual value, satisfactory value, and disallowed value of the ith evaluation index, respectively.

The total efficacy coefficient D_i is calculated by Eq. (16).

$$D_i = \sum_1^n \omega_i \sqrt{\prod_1^n d_i^{\omega_i}}, \tag{16}$$

The total efficacy coefficients of the CA and LCAM were calculated, as indicated in Fig. 22. Compared to the OCA and OCA-prepared LCAM, the D_i of the HCA and HCA-prepared LCAM increased by 49.2% and 10.3%, respectively, indicating that both the HCA and HCA-prepared LCAM developed in this study demonstrated superior comprehensive performance. The high light transmittance and spectral reflectance of the HCA are beneficial for expanding pavement function. The HCA-prepared LCAM had high moisture resistance, and its low-temperature crack resistance was highly prominent, which is beneficial for prolonging the service life of light-colored or colored pavements in rainy or severely cold areas.

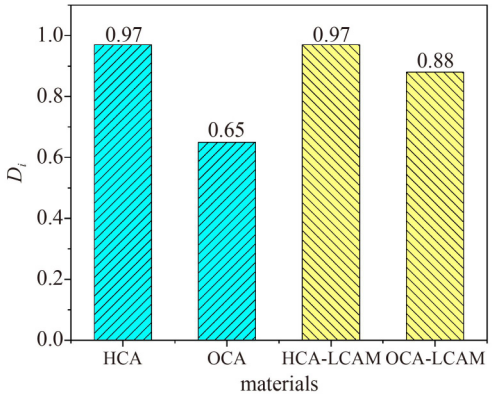

Fig. 22 Total efficacy coefficient.

5 Conclusions

In this study, NO, C5, KH550, and other materials were used to prepare CA with high transparency and adhesion. In addition, LCAM was prepared using HCA and LM aggregates. The physical, chemical, UV aging resistance, and mechanical properties of the CA were characterized; the road performance of the LCAM was evaluated and the economic cost and comprehensive performance of the materials were analyzed. The conclusions of this study are summarized below.

The optimal formulation of high-transparency bitumen determined using the orthogonal test was $m_{NO} : m_{C5}$ = 48:52 + 4%SBS + 2%AO + 0.5%DF. The coupling effect of KH550 improved the HCA adhesion. However, the dilution effect led to a decrease in the hardness and softening point of the HCA. The optimum content of KH550 was 1%.

The transmittance of the 4 mm thick HCA at 580 nm achieved 69.05%, which was 123.30 times greater than that of OCA, and the spectral reflectance of HCA was 3.74 times that of OCA, which is conducive to alleviating the UHI. After UV aging for 144 h, the average *CMAI* and *CVAI* of the HCA were 48% and 53% less than those of the OCA, respectively, owing to the high spectral reflectance of the HCA and chemical influence of the antioxidants.

The FTIR results indicate that certain chemical reactions occurred during the preparation of the HCA. SEM and macroscopic mechanical tests revealed that the SBS modifier formed a network structure in the HCA, which led to changes in the HCA morphology and improved its low-temperature ductility. In addition, HCA had a lower T_g and enthalpy and higher low-temperature crack resistance and thermal stability than OCA.

At the optimum content of KH550, the HCA adhesion considerably improved, and the *MSR*, *TSR*, and low-temperature flexural strain of the LCAM increased by 12.92%, 25.06%, and 23.90%, respectively, compared to those before modification with KH550. However, with the decrease in the hardness and softening point of the

HCA after KH550 modification, the rutting resistance of the HCA-prepared LCAM was 14.3% less than that of the OCA-prepared LCAM. The CA-type had a limited effect on the skid resistance of the LCAM. Therefore, colorless anti-rutting agents could be used to improve the rutting resistance of the LCAM in future studies.

The costs of the HCA and HCA-prepared LCAM were 10.6% and 9.5% greater than those of the OCA and OCA-prepared LCAM, respectively. However, owing to the superior transparency and road performance of the HCA and LCAM, the comprehensive performances were improved by 34.7% and 10.2%, respectively. This research was mainly based on laboratory tests. Practical road engineering should be constructed in the future to investigate the aesthetic, optical, environmental, and road performance of the material.

References

1. Grilli A, Bocci M, Virgili A, Conti C. Mechanical characterization and chemical identification of clear binders for road surface courses. Advances in Materials Science and Engineering, 2020, 2020: 1−9
2. Asif S A, Ahmad N. Comparative study of various properties of clear binder with traditional black binder. Arabian Journal for Science and Engineering, 2022, 47(10): 12979−12991
3. Sengoz B, Bagayogo L, Oner J, Topal A. Investigation of rheological properties of transparent bitumen. Construction & Building Materials, 2017, 154: 1105−1111
4. Xu W, Luo R, Zhang K, Feng G, Zhang D. Experimental investigation on preparation and performance of clear asphalt. International Journal of Pavement Engineering, 2018, 19(5): 416−421
5. Airey G D, Mohammed M H, Fichter C. Rheological characteristics of synthetic road binders. Fuel, 2008, 87(10−11): 1763−1775
6. Rocha Segundo I, Landi S Jr, Margaritis A, Pipintakos G, Freitas E, Vuye C, Blom J, Tytgat T, Denys S, Carneiro J. Physicochemical and rheological properties of a transparent asphalt binder modified with nano-TiO_2. Nanomaterials (Basel, Switzerland), 2020, 10(11): 2152
7. Navarro F J, Partal P, Martínez-Boza F, Gallegos C. Effect of composition and processing on the linear viscoelasticity of synthetic binders. European Polymer Journal, 2005, 41(6): 1429−1438
8. Pasetto M, Baliello A, Giacomello G, Pasquini E. Aesthetic and mechanical suitability of a clear synthetic resin as a unconventional binder for road pavements. Advances in Materials Science and Engineering, 2019, 2019: 1−15
9. Murray R E, Jenne S, Snowberg D, Berry D, Cousins D. Techno-economic analysis of a megawatt-scale thermoplastic resin wind turbine blade. Renewable Energy, 2019, 131: 111−119
10. Merusi F, Giuliani F. Chromatic and rheological characteristics of clear road binders. Transportation Research Record: Journal of the Transportation Research Board, 2012, 2293(1): 114−122
11. Petrukhina N N, Bezrukov N P, Antonov S V. Preparation and use of materials for color road pavement and marking. Russian Journal of Applied Chemistry, 2021, 94(3): 265−283
12. Wu J M, Zhang H C, Qin Z, Wang Z N, Liu J Q, Wang H W, Feng X M, Zhang Y P, Jiao X D, Luo Y. A Light Color Epoxy Asphalt and Its Preparation and Application. CN114230968A, 2022-03-25 (in Chinese)
13. Yan G J, Shi S D, Yuan Y, Xu Y, Yu C Z, Ma Z L, Deng G M, Qiu Y, Xu Y C, Huang Z T, Shi J, Li J, Wang T F, Xia Q Y, Zhou W W, Chen T, Song J, Zhang H G. Transparent Binder for Pavement and Its Preparation Method. CN107674447A, 2018-02-09 (in Chinese)
14. Seo A, Morikubo M, Inoue M, Ozeki N. Colourless and transparent binder. International Publication Number. WO 09/010582A1, 2009-01-22
15. Tang P, Mo L, Pan C, Fang H, Javilla B, Riara M. Investigation of rheological properties of light colored synthetic asphalt binders containing different polymer modifiers. Construction & Building Materials, 2018, 161: 175−185
16. Lee H, Kim Y. Laboratory evaluation of color polymer concrete pavement with synthetic resin binder for exclusive bus lanes. Transportation Research Record: Journal of the Transportation Research Board, 2007, 1991(1): 124−132
17. Bocci E, Bocci M. Clear asphalt concrete for energy saving in road tunnels. In: Proceedings of the 12th International Conference on Asphalt Pavements (ISAP). Raleigh: TRB, 2014, 1817−1825
18. Tang X D, Tan X X, Hu X Y. Pavement performance of colored asphalt modified with titanate coupling agent. Highway, 2017, 62(4): 3 (in Chinese)
19. Yang Y Q, Tang X D, Tan X X, Hu X Y, Xue J L, Guo B. Pavement performance of colored asphalt concrete modified with silane coupling agent. Highway, 2018, 63(7): 4 (in Chinese)
20. JTG E42-2005. Test Methods of Aggregate for Highway Engineering. Beijing: China Communications Press Co., Ltd., 2005 (in Chinese)
21. JTG F40-2004. Technical Specifications for Construction of Highway Asphalt Pavements. Beijing: China Communications Press Co., Ltd., 2004 (in Chinese)
22. JTG E20-2011. Standard Test Methods of Bitumen and Bituminous Mixtures for Highway Engineering. Beijing: China Communications Press Co., Ltd., 2011 (in Chinese)
23. GB/T 32984-2016. Color Asphalt Concrete. Beijing: China Quality and Standards Publishing and Media Co., Ltd., 2016 (in Chinese)
24. Sun L, Xin X, Ren J. Asphalt modification using nano-materials and polymers composite considering high and low temperature performance. Construction & Building Materials, 2017, 133: 358−366
25. Cheng H, Wang F, Ou J, Li W, Xue R. Solar reflective coatings with luminescence and self-cleaning function. Surfaces and Interfaces, 2021, 26: 101325
26. GB/T 17683.1-1999, Solar energy-Reference solar spectral irradiance at the ground at different receiving conditions—Part 1: Direct normal and hemispherical solar irradiance for air mass 1,5. Beijing: China Quality and Standards Publishing and Media Co., Ltd., 1999 (in Chinese)

27. Hossain Z, Bairgi B, Belshe M. Investigation of moisture damage resistance of GTR-modified asphalt binder by static contact angle measurements. Construction & Building Materials, 2015, 95: 45−53
28. Lou K, Kang A, Xiao P, Wu Z, Li B, Wang X. Effects of basalt fiber coated with different sizing agents on performance and microstructures of asphalt mixture. Construction & Building Materials, 2021, 266: 121155
29. Zhang A. Research on anti-UV aging performance of recycled asphalt with waste vegetable oil. Thesis for the Master's Degree. Beijing: Beijing University of Civil Engineering and Architecture, 2018 (in Chinese)
30. AASHTO T315. Standard Method of Test for Determining the Rheological Properties of Asphalt Binder Using a Dynamic Shear Rheometer (DSR). Washington, D.C.: American Association of State Highway and Transportation Officials, 2012
31. JTG 3450-2019. Field Test Methods of Highway Subgrade and Pavemnet. Beijing: China Communications Press Co., Ltd., 2019
32. Xie N, Wang H, Feng D. Coating materials to increase pavement surface reflectance. Eco-efficient Materials for Mitigating Building Cooling Needs. Amsterdam: Elsevier Ltd., 2015, 13−35
33. Lyu L, Pei J, Hu D, Fini E H. Durability of rubberized asphalt binders containing waste cooking oil under thermal and ultraviolet aging. Construction & Building Materials, 2021, 299: 124282
34. Zhao X, Wang S, Wang Q, Yao H. Rheological and structural evolution of SBS modified asphalts under natural weathering. Fuel, 2016, 184: 242−247
35. Omairey E L, Zhang Y, Gu F, Ma T, Hu P, Luo R. Rheological and fatigue characterisation of bitumen modified by anti-ageing compounds. Construction & Building Materials, 2020, 265: 120307
36. Hu M, Ling S, Sun D, Lu T, Ma J, Sun Y. A sustainable high-viscosity modified asphalt modified with multiple anti-aging agents: Micro-chemical analysis and macro-rheological characterization. Construction & Building Materials, 2022, 339: 127701
37. Gürü M, Çubuk M K, Arslan D, Farzanian S A, Bilici I. An approach to the usage of polyethylene terephthalate (PET) waste as roadway pavement material. Journal of Hazardous Materials, 2014, 279: 302−310
38. Zhang Z, Huang Z, Zhou W, Xu R, Xu J, Liu Y. Study on synthesis and road performance of light-colored resin modified asphalt. IOP Conference Series: Earth and Environmental Science, 2021, 770(1): 012003
39. Wang D, Liu Q, Yang Q, Tovar C, Tan Y, Oeser M. Thermal oxidative and ultraviolet ageing behaviour of nano-montmorillonite modified bitumen. Road Materials and Pavement Design, 2021, 22(1): 121−139
40. Koh Y P, Simon S L. Enthalpy recovery of ultrathin polystyrene film using Flash DSC. Polymer, 2018, 143: 40−45
41. Li J, Zhang F, Liu Y, Muhammad Y, Su Z, Meng F, Chen X. Preparation and properties of soybean bio-asphalt/SBS modified petroleum asphalt. Construction & Building Materials, 2019, 201: 268−277
42. JTG 5421-2018. Specification for Maintenance Design of Highway Asphalt Pavement. Beijing: China Communications Press Co., Ltd., 2018 (in Chinese)
43. Hao P, Yuan Y. Development and technical Performance Research of Color Binder. Highway, 2000, 1: 50–51+59 (in Chinese)
44. Chen Q, Wang C, Wen P, Wang M, Zhao J. Comprehensive performance evaluation of low-carbon modified asphalt based on efficacy coefficient method. Journal of Cleaner Production, 2018, 203: 633−644
45. Chen Q, Wang C, Wen P, Sun X, Guo T. Performance evaluation of tourmaline modified asphalt mixture based on grey target decision method. Construction & Building Materials, 2019, 205: 137−147